ACS APPLIED MATERIALS & INTERFACES

Research Article

www.acsami.org

Mitochondria-Targeted Chimeric Peptide for Trinitarian Overcoming of Drug Resistance

Kai Han,[†] Jing-Yi Zhu,[‡] Hui-Zhen Jia,[‡] Shi-Bo Wang,[‡] Shi-Ying Li,[‡] Xian-Zheng Zhang,*[,‡] and He-You Han*[,†]

[†]State Key Laboratory of Agricultural Microbiology, College of Science, Huazhong Agricultural University, Wuhan 430070, China

[‡]Key Laboratory of Biomedical Polymers of Ministry of Education & Department of Chemistry, Wuhan University, Wuhan 430072, China

Supporting Information

ABSTRACT: In this report, an amphiphilic mitochondria-targeted chimeric peptide-based drug delivery system (DDS) was designed to overcome drug resistance. In vitro studies revealed that chimeric peptide could encapsulate doxorubicin (DOX) with high efficacy and target tumor mitochondria, realizing controlled release of DOX and in situ photodynamic therapy (PDT) in mitochondria. Importantly, reactive oxygen species (ROS) during PDT significantly disrupted mitochondria, leading to a dramatic decrease of intracellular adenosine 5′-triphophate (ATP). As a result, ATP-dependent efflux of DOX was remarkably inhibited. Trinitarian therapeutic strategy was developed to ablation of drug-resistant cells, that is, (1) enhanced cellular uptake of hydrophobic DOX via encapsulation in DDS, (2) combined chemo-/photodynamic therapies, and (3) suppressed generation of intracellular ATP as well as drug efflux via in situ PDT in mitochondria. This trinitarian strategy may open a new window in the fabrication of subcellular organelle destructive DDS in overcoming drug resistance.

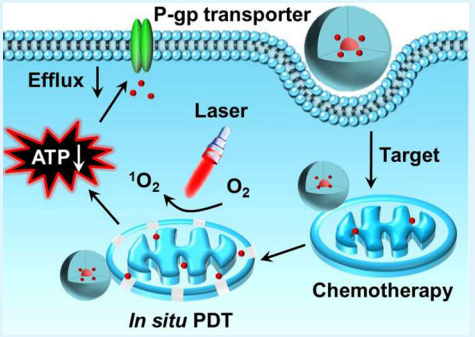

KEYWORDS: *ATP, mitochondria disruption, photodynamic therapy, drug resistance, combined therapy*

1. INTRODUCTION

Traditional chemotherapy always suffers from the barrier of drug resistance.[1−3] Drug resistance is a very complex phenomenon, and overexpressed ATP-binding cassette (ABC) transporters in tumor have been recognized to play a crucial role in drug resistance.[4,5] ABC transporters can pump hydrophobic substrates actively from the cell cytosol or membrane to the extracellular space via an ATP-dependent manner, which will remarkably decrease intracellular drug content.[6,7] In other words, drug-resistant tumor cells can survive from cytotoxic damage of antitumor drugs, resulting in failure of chemotherapy. To overcome this dilemma, various elegant drug delivery systems (DDSs) have been developed. Generally, these DDSs can improve the chemical stability of antitumor drugs, achieve sustained drug release, facilitate cellular uptake, and reduce drug efflux in tumor cells.[8,9] Moreover, these DDSs can also realize combined therapies among various drugs or/and genetic materials with ease.[10,11] Although great success has been achieved, traditional DDSs in overcoming drug resistance still face several challenges: drug carriers are always excipients. The low drug loading capacity requires higher doses of carriers, which may cause severe potential systemic toxicity.[12] On the other hand, repeated administration of various drugs simultaneously can still arouse acquired drug resistance especially for long-term treatment.[13] Most importantly, the majority of current DDSs release drugs in cytoplasm.[14,15] Free diffusion of drugs to traditional targets including nuclei is time-consuming. During this processing, drugs can be actively pumped out of cells via ABC transporters, which compromises therapeutic efficacy inevitably.[16,17] So far, great efforts have been devoted to develop nucleus-targeted DDSs to overcome drug resistance.[18−20] However, fabrication of these DDSs is arduous due to the small size of the nuclear pore (around 9−40 nm).[21] Meanwhile, small enough DDSs may undergo rapid metabolic clearance and minimal accumulation in tumor. Hence, construction of easy-to-fabricate DDSs with a novel suppression pathway in drug resistance is still very challenging and highly urgent.

Recently, mitochondria-targeted DDSs have rapidly obtained considerable attention, because mitochondria are the decisive regulators in intrinsic pathway of apoptosis.[22−24] Meanwhile, mitochondria are widely spread in cytoplasm, and drugs can be delivered to mitochondria without overcoming additional hurdles such as karyotheca, which can remarkably simplify the preparation of DDSs.[25] Unfortunately, most of the previous work focuses on mitochondria-targeted drug release. DDSs with mitochondrial specific damage aiming at overcoming drug resistance have been rarely reported. It is recognized that

Received: May 31, 2016
Accepted: September 6, 2016
Published: September 6, 2016

DOI: 10.1021/acsami.6b06522
ACS Appl. Mater. Interfaces 2016, 8, 25060−25068

mitochondrion is the energy center of cells, which manipulates the generation of intracellular ATP.[26] Specially, active drug efflux mediated by efflux transporter is mainly ATP-dependent.[27,28] Therefore, we hypothesize that mitochondrial specific damage may suppress active drug efflux.

As a proof of concept, we developed a mitochondria-targeted chimeric peptide (denoted as MTCP), protoporphyrin IX-6-aminohexanoic acid-PEG$_{8-d}$(Lys-Leu-Ala-Lys-Leu-Ala-Lys)$_2$-Gly-Arg-Gly-Asp (PpIX-Ahx-PEG$_{8-d}$(KLAKLAK)$_2$-GRGD), for combined chemo-/photodynamic therapies to overcome drug resistance. As shown in Figure 1, amphiphilic MTCP

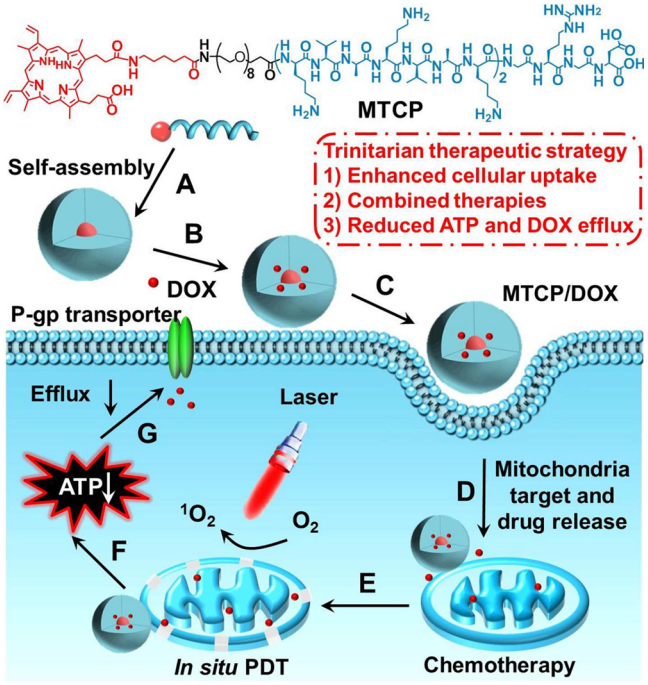

Figure 1. Chemical structure of MTCP and schematic illustration of trinitarian inhibition of drug resistance in tumor cells: (A) Self-assembly of MTCP; (B) encapsulation of DOX; (C) internalization of MTCP/DOX; (D) $_d$(KLAKLAK)$_2$-mediated mitochondria-targeted accumulation of MTCP/DOX and controlled release of DOX; (E) in situ PDT in mitochondria and the consequent mitochondrial destruction; (F) decreased generation of intracellular ATP; and (G) suppressed efflux of DOX.

could encapsulate hydrophobic DOX and improve cellular internalization via formation of MTCP/DOX nanoparticles. Meanwhile, different from traditional DDSs with low drug loading efficacy, MTCP contained both photosensitizer PpIX and biodrug $_d$(KLAKLAK)$_2$;[29] the resulting MTCP/DOX owned an extremely high drug/carrier mass ratio, which could significantly decrease dosage and achieve combined chemo-/photodynamic therapies. Importantly, both proapoptosis peptide $_d$(KLAKLAK)$_2$-mediated mitochondrial target/disruption and in situ PDT in mitochondria dramatically decreased intracellular ATP generation, which resulted in inhibited efflux of DOX. For the first time, we proposed a trinitarian therapeutic strategy to overcome drug resistance, and the efficacy was assessed in terms of cytotoxicity, drug efflux, and so on.

2. EXPERIMENTAL SECTION

2.1. Materials. DOX·HCl was from Zhejiang Hisun Pharmaceutical Co. (China). Fmoc-Ahx-COOH, 2′,7′-dichlorofluorescin diacetate (DCFH-DA), and MitoTracker Green were provided from Sigma-Aldrich, and Fmoc-PEG$_8$-COOH was purchased from Qiancheng Technology Co. (Hangzhou, China). More detailed material information could be found in our previous work.[30]

2.2. Peptide Synthesis. MTCP was synthesized in a stepwise manner.[31] Briefly, MTCP was loaded on 2-chlorotrityl chloride resin. HBTU/HOBT/DIEA was employed to accelerate coupling efficacy of amino acids. Also, 20% piperdine/DMF was employed to deprotect the Fmoc group two times (10 + 10 min). A mixed solution of triisopropylsilane, H_2O, and trifluoroacetic acid (volume ratio: 2.5:2.5:95) was used to detach MTCP from resin for 1.5 h. Peptide was precipitated in ether. Subsequently, it was collected and dried in a vacuum. The molecular weight of MTCP was recorded via matrix-assisted laser desorption/ionization time-of-flight mass spectrometry (MALDI-TOF-MS).

2.3. Size and Morphology Observation. The hydrodynamic sizes of MTCP and MTCP/DOX were measured via a Nano-ZS ZEN3600. For stability study, hydrodynamic sizes of MTCP/DOX at 4, 8, and 12 h were recorded. Morphology of MTCP and MTCP/DOX was observed via a transmission electron microscope (TEM) machine. MTCP was 100 mg/L.

2.4. Circular Dichroism (CD). The secondary structure of MTCP was tested via a J-810 spectropolarimeter (Jasco, Japan). MTCP was 100 mg/L. The spectrum was scanned from 270 to 180 nm three times.

2.5. Intracellular ROS Measurement. The intracellular ROS detection was conducted as in our previous report.[32] Briefly, HeLa cells were cultured with different samples (MTCP, 50 mg/L; free PpIX in DMEM supplemented with 2.5% DMSO, 9.4 mg/L). Cells were repeatedly washed with PBS buffer after incubation for 4 h. Medium was then replaced with DMEM supplemented with DCFH-DA (ROS sensor, final concentration: 1×10^{-5} M). Twenty minutes later, cells were washed with PBS buffer thoroughly to remove residual DCFH-DA and received 10 min of light irradiation (3.3 mW/cm^2, band-pass: 400−700 nm). Cells were observed via confocal laser scanning microscopy (CLSM). 2′,7′-Dichlorofluorescin (DCF) was excited with an argon laser (488 nm). Quantitative analysis of fluorescence intensity was conducted via ImageJ software.

2.6. Cellular Internalization. Human cervical carcinoma (HeLa) and African green monkey SV40-transfected kidney fibroblast (COS7) cells were incubated in 6-well plates. After 24 h of incubation, 50 mg/L MTCP in 10% FBS medium was added. Cells were cultured for 4 h. Thereafter, cell nucleus was stained by Hoechst 33342 (20 μL, 2 μg/μL in DMEM medium) solution. Fifteen minutes later, residual Hoechst 33342 was removed with PBS buffer washing, and then the samples were imaged directly via CLSM.

2.7. Mitochondrial Colocalization. HeLa cells were seeded in a 6-well plate. After 24 h of incubation, 50 mg/L MTCP in 10% FBS medium was added. Cells were cultured for 4 h. Thereafter, mitochondria were stained by MitoTracker Green solution (10 μL, 2 mg/mL in DMEM) for 30 min. Residual MitoTracker Green was removed with PBS buffer washing, and then samples were imaged directly via CLSM. The emission at 600−700 nm was recorded for MTCP, and the emission at 500−550 nm was recorded for MitoTracker Green.

2.8. Determination of Mitochondrial Membrane Potential. CLSM was used to determine the change of mitochondrial membrane potential. Briefly, after 24 h of incubation, 40 mg/L MTCP in 10% FBS was added to HeLa cells. Sample was extracted, and cells were repeatedly washed after 4 h of incubation. Subsequently, different light irradiation times (0, 15, and 30 min) were performed (3.3 mW/cm^2, band-pass: 400−700 nm). Cells were further cultured for 30 min. Thereafter, 2.5 mg/L of JC-1 was used to stained mitochondria for 30 min. Free JC-1 was removed via repeatedly washing with PBS. The excitation wavelength was chosen at 488 nm. The fluorescence emissions at 510−540 nm (monomeric JC-1) and at 570−600 nm (aggregated JC-1) were collected. Pearson's correlation coefficient was calculated via ImageJ software.

2.9. Drug Loading and Release. MTCP (10 mg) and DOX (2 mg) were dissolved in the mixture of DMSO (3 mL) supplement with

DOI: 10.1021/acsami.6b06522
ACS Appl. Mater. Interfaces 2016, 8, 25060−25068

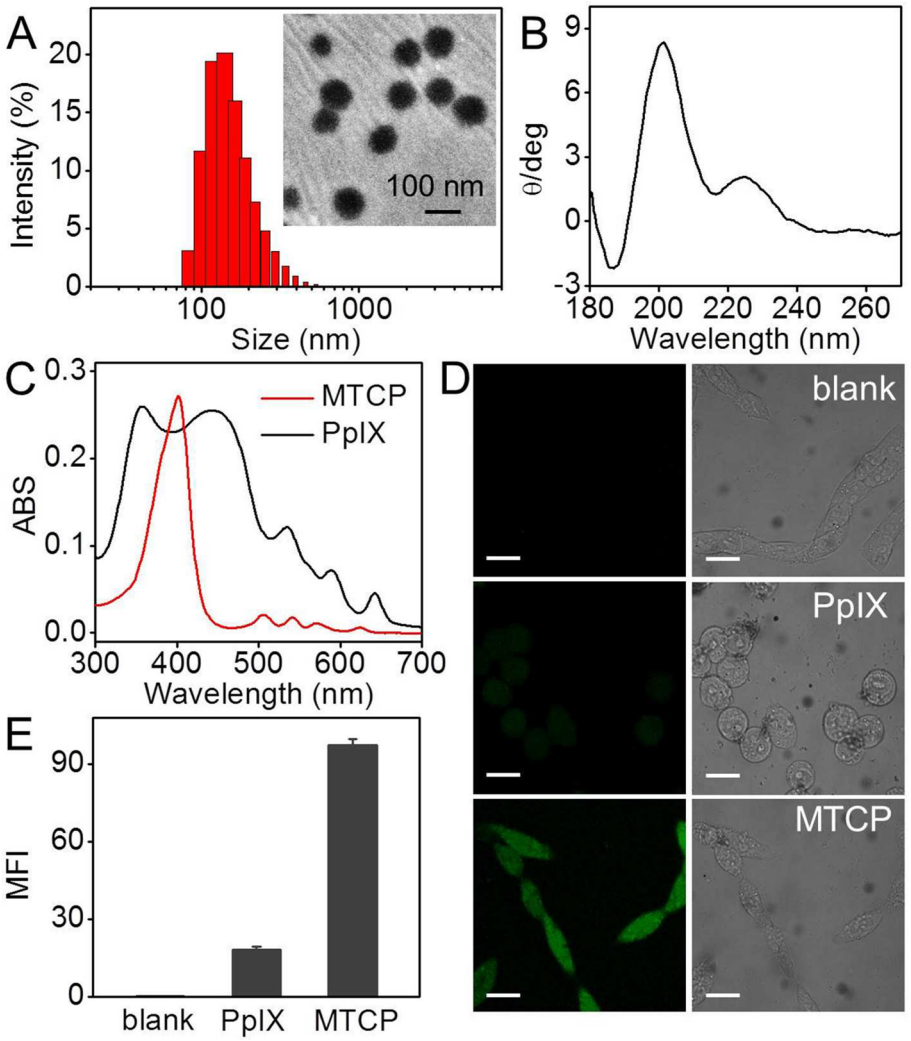

Figure 2. (A) Hydrodynamic size, inset was the corresponding TEM image, (B) CD spectrum, and (C) UV−vis spectrum of MTCP. (D) Intracellular ROS generation in blank HeLa cells, PpIX-treated cells, and MTCP-treated cells, respectively. Green signal: DCF. The scale bar was 10 μm. (E) Mean fluorescence intensity of DCF in HeLa cells.

triethylamine (0.6 mL). After 12 h of being stirred, the solution was dialyzed. The dialysis tube (MWCO 1000 Da) was subjected to PBS buffer (pH 7.4), and PBS buffer was replaced every 4 h to load DOX. After dialysis for 24 h, some solution was lyophilized to determine drug loading efficiency (DLE) and encapsulation efficiency (EE) values via UV−vis spectrum. The residue solution was put into the dialysis tube and then immersed into PBS buffer (10 mL, pH 7.4) for in vitro drug release evaluation. The solution was replaced with the same volume of PBS buffer periodically. The amount of released DOX was also measured via UV−vis spectrum. The release of free DOX·HCl in PBS buffer was used as a control. EE and DLE were calculated as the following formulas:

$$\text{EE value} = (\text{mass of encapsulated DOX in MTCP}/\text{mass of DOX fed initially}) \times 100\%$$

$$\text{DLE value} = (\text{mass of encapsulated DOX in MTCP}/\text{mass of DOX} - \text{encapsulated MTCP}) \times 100\%$$

2.10. In Vitro Cytotoxicity. MTT assay was employed to test the cytotoxicity against human breast carcinoma (MCF-7) cells as well as DOX-resistant human breast carcinoma (MCF-7/ADR) cells, respectively. Briefly, after the seeding of cells on 96-well plates for 24 h, samples with various concentrations were added. Samples were replaced with fresh culture medium after 4 h of incubation. For phototoxicity, light irradiation was performed (3.3 mW/cm^2, band-pass: 400−700 nm). After 48 h of incubation, 20 μL of MTT (5 mg/mL) was added. The medium containing MTT was extracted after 4 h of incubation, and DMSO was added. OD values at 490 nm were determined. The following formula was employed to calculate the cell viability: cell viability (%) = $OD_{(sample)}/OD_{(control)} \times 100\%$.

2.11. Combination Index Determination. CI was calculated as $CI_x = D_1/Df_1 + D_2/Df_2$. D_1 or D_2 was defined as the required dose of drug 1 or drug 2 to mediate the x percent cell death. Df_1 or Df_2 was defined as the required dose of drug 1 or drug 2 to mediate the x percent cell death alone, respectively.

2.12. Drug Internalization and Efflux Measurement. MCF-7/ADR cells and MCF-7 cells were incubated on 6-well plates for 24 h. For DOX internalization, MTCP/DOX and free DOX (4 μg/mL DOX in PBS) were added, respectively. Four hours later, cells were thoroughly washed, and to each well was added 0.5 mL of trypsin. The suspension cells were collected and counted. Thereafter, cells were repeatedly freeze−thawed and sonicated on crushed ice for 5 min. Cells were centrifuged for 4 min at 3000 r/min, and a fluorescence spectrum was conducted to detect DOX amount. For efflux study, after 4 h of incubation with various samples, a part of the MCF-7/ADR cells and MCF-7 cells was collected to detect the initial internalization amount of DOX via fluorescence spectrum. The other MCF-7/ADR cells and MCF-7 cells were replaced with fresh culture medium. To test the influence of light irradiation, preset times of light

DOI: 10.1021/acsami.6b06522
ACS Appl. Mater. Interfaces 2016, 8, 25060−25068

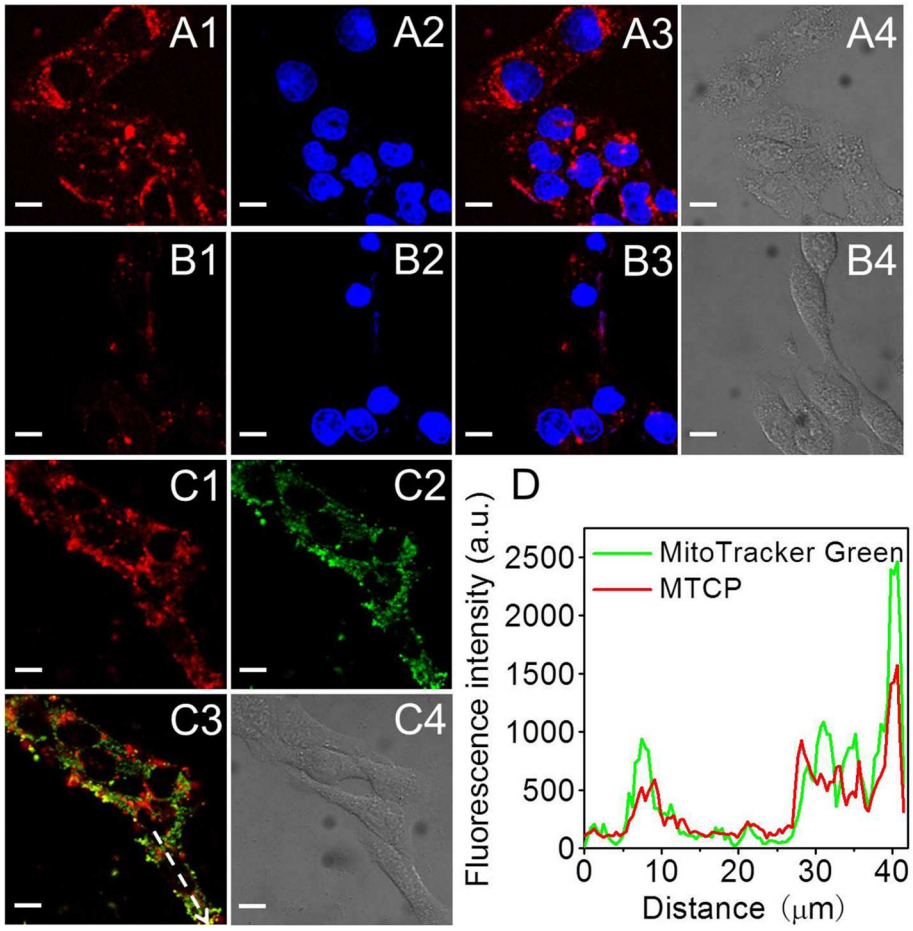

Figure 3. Cellular uptake of MTCP in (A1-A4) HeLa cells and (B1−B4) COS7 cells. Red signal, MTCP; blue signal, Hochest 33342 stained nucleus; A3, B3, merged field; A4, B4, bright field. (C) Mitochondria targeting observation of MTCP and (D) the fluorescence intensity profile analysis of MitoTracker Green and MTCP (red), across the arrowed line. Green signal: MitoTracker Green. The scale bar was 10 μm.

irradiation were performed after cells were replaced with fresh culture medium. Cells then were cultured for 18 h. After washing with PBS, cells were collected to detect the final concentration of DOX via fluorescence spectrum. The efflux amount of DOX was calculated via subtracting the final amount of DOX from the initially internalized amount of DOX.

2.13. Intracellular ATP Generation. ATP bioluminescent assay kit (Sigma-Aldrich) was used to determine the cellular ATP levels. Various samples including free DOX and MTCP/DOX (40 mg/L) were added to MCF-7/ADR cells. Four hours later, samples were replaced with fresh medium, and MTCP/DOX-treated cells further received 0, 15, and 30 min light irradiation, respectively. Subsequently, cells were treated with lysis buffer before being washed with PBS. ATP level was measured according to the protocol of ATP bioluminescent assay kit.

2.14. Western Blotting Analysis. The expression level of P-gp protein was measured via Western blotting. MCF-7/ADR cells were incubated for 24 h. Samples including free DOX and MTCP/DOX (40 mg/L) then were added. Four hours later, samples were replaced with fresh medium. Thereafter, MTCP/DOX treated cells received 0, 15, and 30 min light irradiation, respectively. Twenty-four hours later, cells were analyzed by Western blotting.

2.15. Statistical Analysis. Statistical analysis among different groups was measured by Student's t test. When the p value < 0.05, it could be considered that there existed statistically significant differences.

3. RESULTS AND DISCUSSION

3.1. Characterization of MTCP. MTCP was synthesized via solid-phase peptide synthesis method. The theoretical molecule weight was 2989.8, while a peak at 2988.8 was found in MALDI-TOF-MS (Figure S1), which confirmed the validity of MTCP. TEM image revealed that MTCP with typical amphiphilic structure self-assembled into uniform, well-dispersed, spherical nanoparticles in aqueous solution (Figure 2A). Dynamic light scattering (DLS) study further indicated that the hydrodynamic size of these nanoparticles was 135 ± 5 nm (Figure 2A). The size observed by DLS was greater than that by TEM; because the TEM observation of MTCP was under the vacuum state, shrinkage of nanoparticles would appear.[33] Given the fact that α-helical conformation of $_{d}$(KLAKLAK)$_2$ was important for mitochondrial target and disruption, the effect of self-assembly on conformation of MTCP was assessed via CD spectrum. As shown in Figure 2B, characteristic peaks at 224, 202, and 187 nm were observed, indicating self-assembly would not affect α-helical conformation of MTCP. Note that because $_{d}$(KLAKLAK)$_2$ was composed of the D enantiomer amino acids, the peak shape of MTCP in CD was mirror symmetry along the X direction, when compared to a typical α-helical peak shape.[29]

In addition, self-assembly behavior of MTCP could significantly improve water solubility of PpIX as well as generation of intracellular ROS. The UV−vis spectrum revealed

DOI: 10.1021/acsami.6b06522
ACS Appl. Mater. Interfaces 2016, 8, 25060−25068

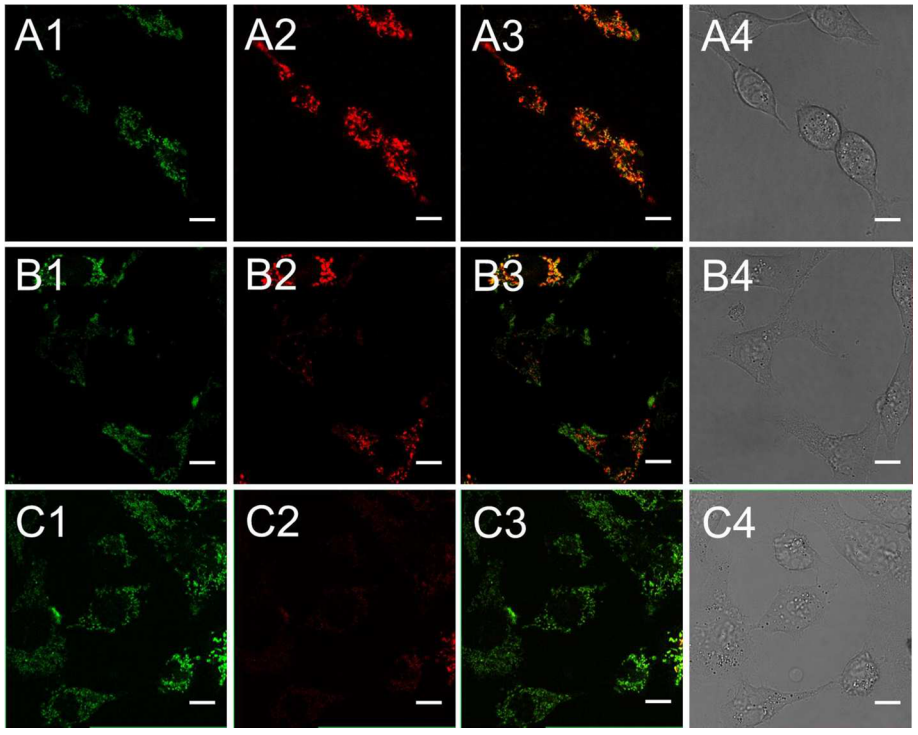

Figure 4. CLSM images of mitochondrial membrane potential change. HeLa cells were incubated with 40 μg/mL of MTCP and received (A1−A4) 0 min, (B1−B4) 15 min, and (C1−C4) 30 min light irradiation. JC-1 was the indicator. Green signal, monomeric JC-1; red signal, JC-1 aggregate; A3−C3, merged images. The scale bar was 10 μm.

that broadened dual-peaks existed in free PpIX solution, while a sharp Soret band was detected in MTCP solution, indicating that $\pi-\pi$ stacking would not mediate significant aggregation in MTCP (Figure 2C).[34] Subsequently, DCFH-DA was used as a ROS sensor to assess ROS generation capacity. It was reported that DCF with green fluorescence would rapidly form when nonfluorescence DCFH-DA met ROS. As shown in Figure 2D, significant green fluorescence appeared when HeLa cells were incubated with MTCP, indicating the formation of intracellular ROS under light irradiation. For comparison, just very weak fluorescence was detected in both blank and PpIX-treated HeLa cells. The corresponding mean fluorescence intensity (MFI) values were also calculated as shown in Figure 2E. Apparently, enhanced water solubility remarkably increased bioactivity of PpIX. Note that different cellular morphology was oberved in PpIX-treated cells (Figure 2D), because DMSO was introduced to improve the solubility of PpIX, which affected the cellular morphology to some extent (Figure S2).

3.2. Tumor Cell and Mitochondria Dual-Target of MTCP. Because the GRGD sequence was introduced to MTCP, MTCP was expected to target tumor cells. To verify it, cellular uptake of MTCP in HeLa and COS7 cell-lines was measured via CLSM. It was found that a significant red signal with large area appeared in HeLa cells, indicating the great internalization of MTCP in HeLa cells (Figure 3A1). In sharp contrast, the red signal in COS7 cells was dramatically decreased (Figure 3B1). For comparison, a negligible difference in cellular uptake of free PpIX was observed between these cell-lines (Figure S3). This difference for MTCP was attributed to different expression levels of $\alpha_v\beta_3$ integrin between these two cell-lines. Unlike normal cells whose $\alpha_v\beta_3$ integrin expression on cell membrane was very limited, $\alpha_v\beta_3$ integrin in many types of tumor cells including HeLa cells was overexpressed. The GRGD sequence could recognize $\alpha_v\beta_3$ integrin specifically, leading to receptor-mediated endocytosis as well as accelerated cellular internalization.

After cellular internalization, the subcellular localization of MTCP was visualized via CLSM. Mitochondria were labeled with MitoTracker Green. As shown in Figure 3C3, the red fluorescence of MTCP could be overlapped well with green fluorescence, which substantially indicated the mitochondria-targeting ability of MTCP. The corresponding Pearson's correlation coefficient (p = 0.51)[35,36] and fluorescence-intensity-profile analysis further confirmed it (Figure 3D). Mitochondrial localization was due to the strong interaction between cationic α-helical $_d$(KLAKLAK)$_2$ and negatively charged mitochondrial membrane. This specifically mitochondrial colocalization provided great opportunity to in situ PDT in mitochondria.

3.3. In Situ PDT-Mediated Destruction of Mitochondria by MTCP. CLSM was employed to measure the PDT-induced damage of mitochondrial. Herein, we chose JC-1 dye as the sensor. It was known that in normal mitochondria with high membrane potential JC-1 keeps aggregated and fluoresces red. While in dysfunctional mitochondria with decreased membrane potential, JC-1 keeps monomeric and fluoresces green.[37] So the red/green fluorescence ratio represented the status of mitochondria to a great extent. As shown in Figure 4A1, some green fluorescence was found when no irradiation was performed. It was due to the existence of cationic proapoptosis $_d$(KLAKLAK)$_2$ sequence in MTCP, which could penetrate and disrupt mitochondrial membrane. Meanwhile, the self-assembly behavior of MTCP could further enhance the destructive power of $_d$(KLAKLAK)$_2$.[38] Besides, it was observed that green fluorescence became stronger while red fluorescence gradually got weaker, when the light irradiation time was

DOI: 10.1021/acsami.6b06522
ACS Appl. Mater. Interfaces 2016, 8, 25060−25068

prolonged from 0 to 15 and 30 min. Obviously, light irradiation could trigger the generation of ROS in mitochondria in situ. ROS damaged mitochondria, leading to significant decrease of membrane potential.

3.4. Trinitarian Inhibition of Drug Resistance. Encouraged by the novel properties of MTCP in tumor/mitochondria target and light-induced mitochondrial disruption, we proceeded to investigate the ability of MTCP in overcoming drug resistance. Before that, the widely used hydrophobic drug DOX was encapsulated by MTCP via classic membrane dialysis method. The obtained MTCP/DOX exhibited a hydrodynamic size of 202.9 ± 36.1 nm (Figure 5A). Hydrodynamic size over

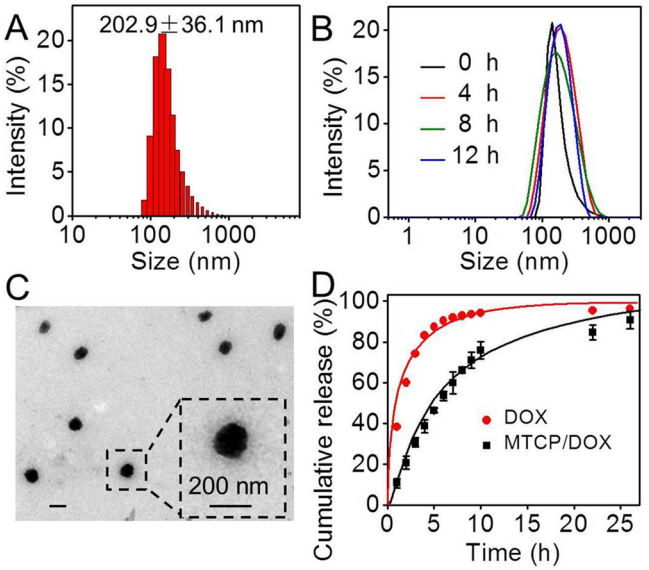

Figure 5. (A) Hydrodynamic size and (B) the corresponding stability of MTCP/DOX with prolonging of incubation time. (C) TEM image of MTCP/DOX. (D) Drug release of DOX from MTCP/DOX at pH 7.4. Free DOX was used as a control.

time confirmed that MTCP/DOX exhibited well stability in aqueous solution (Figure 5B). TEM image revealed that uniformly spherical nanoparticles formed (Figure 5C), and encapsulation of DOX enlarged the size of MTCP, suggesting the successful loading of DOX.[39,40] MTCP/DOX exhibited high a EE value (34.9%) and DLE value (14.0%). Specifically, MTCP/DOX kept an extremely high drug/carrier mass ratio (DOX and $_d$(KLAKLAK)$_2$: carrier), which was up to 85.5%. The high DLE value was due to the following facts: introduction of hydrophobic alkyl chain improved the flexibility of MTCP and the hydrophobic interaction between MTCP and DOX. On the other hand, both electrostatic interaction and $\pi-\pi$ stacking interaction between PpIX and DOX further stabilized MTCP/DOX. The drug releasing curve revealed that DOX could be gradually liberated from MTCP nanoparticles, when compared to free DOX. 76% DOX was released from MTCP nanoparticles at the 10th hour (Figure 5D). CLSM results indicated that MTCP/DOX exhibited a time-dependent cellular uptake (Figure S4).

To test the feasibility of MTCP/DOX in trinitarian inhibition of drug resistance, cytotoxicity was measured via MTT assay. We chose broadly used MCF-7/ADR cells and MCF-7 cells as cell models. Different from the severe toxicity in MCF-7 cells, DOX could not efficiently kill MCF-7/ADR cells even when the concentration of DOX was 100 mg/L (Figure S5A). As shown in Figure 6A, in MCF-7 cells, MTCP had a certain cytotoxicity due to the existence of biodrug $_d$(KLA-

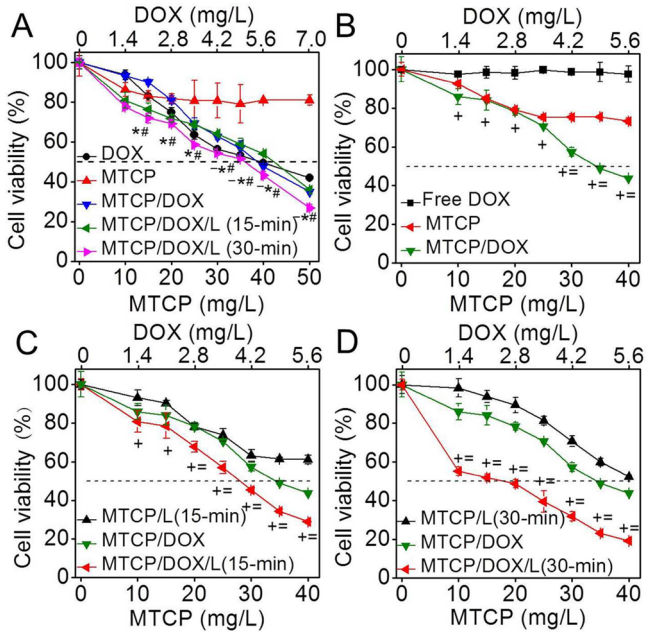

Figure 6. Cytotoxicity of various samples in vitro via MTT assay: (A) DOX, MTCP, MTCP/DOX with 0, 15, and 30 min light irradiation against MCF-7 cells. ^{-}p, $^{*}p$, and $^{\#}p < 0.05$, when MTCP/DOX-treated MCF-7 cells with 30 min light irradiation was compared to cells treated with MTCP/DOX with 15 min light irradiation, MTCP and MTCP/DOX. (B) DOX, MTCP, MTCP/DOX without light irradiation against MCF-7/ADR cells; (C) MTCP or MTCP/DOX with 15 min light irradiation against MCF-7/ADR cells; (D) MTCP or MTCP/DOX with 30 min light irradiation against MCF-7/ADR cells. "L" represented light irradiation. ^{+}p and $^{=}p < 0.001$, when the group was compared to cells treated with MTCP/DOX and MTCP with 30 min light irradiation.

KLAK)$_2$ and inherent dark-toxicity of PpIX. The IC$_{50}$ (the concentration that inhibited 50% cellular growth) of MTCP was 94.9 mg/L (Figure S5B). MTCP/DOX exhibited elevated toxicity (IC$_{50}$: 38.7 mg/L). Also, light irradiation could increase cytotoxicity (IC$_{50}$ for MTCP/DOX with 30 min light irradiation: 35.9 mg/L). Note that the toxicity of MTCP/DOX was somewhat lower than that of free DOX (IC$_{50}$ for DOX: 6.2 mg/L, Figure S5A), because the release of DOX was time-consuming. In MCF-7/ADR cells, similar results were observed that MTCP still performed limited toxicity. Meanwhile, MTCP/DOX (without light irradiation) significantly enhanced the cell toxicity to MCF-7/ADR cells (Figure 6B). These results were in agreement with a previous report.[41] Clearly, formation of MTCP/DOX improved internalization of DOX in MCF-7/ADR cells. Meanwhile, controlled drug release also avoided efflux of DOX via P-gp transporter to some extent.

To demonstrate the influence of PDT on drug resistance, MCF-7/ADR cells received 15 min light irradiation after cellular endocytosis. As a drug carrier, MTCP showed a certain phototoxicity even in MCF-7/ADR cells (Figure 6C). Importantly, MTCP/DOX with 15 min of light irradiation induced the greatest toxicity to MCF-7/ADR cells, when compared to both MTCP with 15 min light irradiation and MTCP/DOX without light irradiation (Figure 6C). Furthermore, we prolonged the irradiation time to 30 min, and the cytotoxicity of MTCP/DOX was further elevated in MCF-7/

DOI: 10.1021/acsami.6b06522
ACS Appl. Mater. Interfaces 2016, 8, 25060−25068

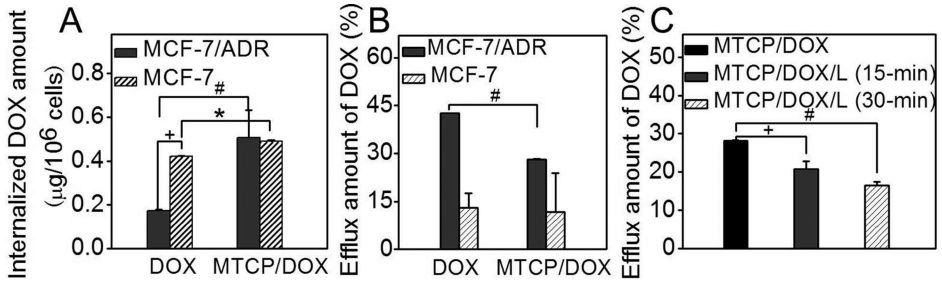

Figure 7. (A) Internalization and (B) efflux amount of DOX in free DOX and MTCP/DOX against MCF-7 and MCF-7/ADR cells. (C) DOX efflux in MTCP/DOX with 0, 15, and 30 min light irradiation against MCF-7/ADR cells. "L" represented light irradiation. ^{+}p, $^{\#}p$, and $^{*}p < 0.05$ were measured by a Student's t test.

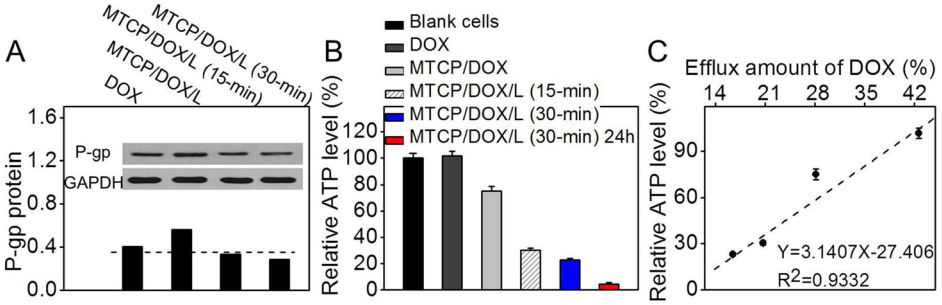

Figure 8. (A) Western blotting analysis of P-gp expression of various samples. GAPDH was used as a control. (B) Relative intracellular ATP level of various samples. (C) Relationship between relative ATP level and efflux amount of DOX. "L" represented light irradiation.

ADR cells (Figure 6D). The IC_{50} values of MTCP with 30 min of light irradiation, and of MTCP/DOX and MTCP/DOX with 30 min of light irradiation, were 41.3, 34.4, and 17.1 mg/L, respectively. The corresponding combination index was less than 1,[42] suggesting that the significantly reduced drug resistance of MTCP/DOX under light irradiation was not just attributed to controlled drug release and the combined chemo-/photodynamic therapies. We believed that in situ PDT in mitochondria specifically disrupted the energy center of mitochondria, which could restrict the energy-dependent active efflux of DOX.

3.5. Cellular Uptake and Efflux of DOX. To further confirm our speculation that in situ PDT restricted drug efflux and intuitively observe the inhibition of drug resistance, the internalization and efflux of DOX were measured, because drug resistance in tumor cells was highly associated with several factors including defective endocytosis and drug efflux by pumps overexpressed on cell membrane.[43,44] As shown in Figure 7A, the internalization amount of free DOX in MCF-7/ADR cells was observably lower than that in MCF-7 cells. Also, MTCP remarkably improved the internalization of DOX in both cell-lines. Meanwhile, a negligible difference was observed in cellular uptake of MTCP/DOX between MCF-7/ADR and MCF-7 cells. All of these results suggested that the formation of MTCP/DOX nanoparticles could enhance drug internalization in drug-resistant tumor cells.

Thereafter, efflux behavior of DOX was studied. It was found that, although the efflux amount of DOX in MTCP/DOX-treated MCF-7/ADR cells was obviously lower than that in free DOX-treated MCF-7/ADR cells (Figure 7B), the efflux amount of DOX in MTCP/DOX-treated MCF-7/ADR cells was still greater than that in MTCP/DOX-treated MCF-7 cells. Similar results were also reported in a previous report,[45] suggesting that encapsulation of drug in MTCP nanoparticles could only inhibit drug efflux to some extent. Subsequently, efflux behavior of DOX in MTCP/DOX-treated MCF-7/ADR cells under light irradiation was presented. Encouragingly, light irradiation further decreased efflux of DOX. Meanwhile, the efflux amount decreased with the prolonging of irradiation time (Figure 7C). The efflux amount of DOX against MCF-7/ADR cells under 30 min of light irradiation could be as low as 16%, which was even comparable to that of MTCP/DOX against MCF-7 cells. The average efflux speed was also performed in Figure S6. These results exhibited a tendency similar to that of cytotoxicity, which substantially demonstrated that satisfactory inhibition of drug resistance by MTCP/DOX under light irradiation was not just due to the traditional and mechanical combination of chemo-/photodynamic therapies, but also PDT-induced inhibition of drug efflux played a crucial role in overcoming drug resistance with high efficacy.

3.6. Mechanism Study of PDT-Induced Inhibition of Drug Resistance. To get direct insight of the mechanism of inhibited drug efflux and resistance, the expression level of P-gp protein in MCF-7/ADR cells was tested. P-glycoprotein (P-gp) was recognized as one of the most important ABC transporters in drug efflux. As shown in Figure 8A, the difference of P-gp protein expression among various groups was not very great via Western blotting analysis, especially for DOX, MTCP/DOX with 15 min light irradiation, and MTCP/DOX with 30 min light irradiation, which indicated that encapsulation of DOX or light irradiation would not severely affect the expression of P-gp protein. Therefore, expression of P-gp protein played an indecisive role in suppression of the efflux of DOX in MTCP/DOX.

Subsequently, an intracellular amount of ATP was detected when MCF-7/ADR cells were incubated with various samples. As shown in Figure 8B, the amount of intracellular ATP decreased in the following order: DOX ≫ MTCP/DOX ≫ MTCP/DOX with 15 min of light irradiation > MTCP/DOX with 30 min of light irradiation. Intracellular ATP amount in

DOI: 10.1021/acsami.6b06522
ACS Appl. Mater. Interfaces 2016, 8, 25060−25068

MTCP/DOX group further decreased when MCF-7/ADR cells got 30 min of light irradiation followed by further incubation for 24 h. It was also noticed that the amount of intracellular ATP exhibited a linear relationship with efflux amount of DOX (Figure 8C), which suggested that the amount of intracellular ATP would largely determine the drug efflux. Taken together, in situ PDT in mitochondria damaged mitochondria, which significantly decreased ATP generation. Decreased ATP generation further inhibited active drug efflux by P-gp transporter, achieving well therapeutic efficacy.

4. CONCLUSION

In summary, a mitochondria-targeted chimeric peptide MTCP was developed for trinitarian overcoming of drug resistance in tumor cells. MTCP could transport DOX to tumor mitochondria and release it in a sustained manner. Meanwhile, the biodrug $_{d}(KLAKLAK)_{2}$ as well as in situ PDT of MTCP in mitochondria destroyed the energy center mitochondria, realizing combined chemo-/photodynamic therapies. Particularly, different from the traditional DDSs, which overcame drug resistance via inhibition, from the expression of efflux transporters or nuclei-targeted drug transportation, MTCP/DOX damaged mitochondria in situ via ROS, resulting in decreased intracellular ATP, which significantly suppressed efflux of DOX in drug-resistant tumor cells. This subcellular organelle specifically damaged strategy should provide a new approach to overcome drug resistance for ablation of resistant tumor cells.

■ ASSOCIATED CONTENT

Supporting Information

The Supporting Information is available free of charge on the ACS Publications website at DOI: 10.1021/acsami.6b06522.

MALDI-TOF-MS of MTCP; morphology of HeLa cells in culture medium supplement with 2.5% DMSO; cellular uptake of free PpIX in HeLa cells and COS7 cells; cellular uptake of MTCP/DOX in HeLa cells over time; and cytotoxicity of MTCP in MCF-7 cells, free DOX in MCF-7/ADR cells, and MCF-7 cells (PDF)

■ AUTHOR INFORMATION

Corresponding Authors

*E-mail: xz-zhang@whu.edu.cn.
*E-mail: hyhan@mail.hzau.edu.cn.

Notes

The authors declare no competing financial interest.

■ ACKNOWLEDGMENTS

This work was financially supported by the Fundamental Research Funds for the Central Universities (2662015QD026) and the National Natural Science Foundation of China (51603080, 21375043, and 21175051).

■ REFERENCES

(1) Crystal, A. S.; Shaw, A. T.; Sequist, L. V.; Friboulet, L.; Niederst, M. J.; Lockerman, E. L.; Frias, R. L.; Gainor, J. F.; Amzallag, A.; Greninger, P.; Lee, D.; Kalsy, A.; Gomez-Caraballo, M.; Elamine, L.; Howe, E.; Hur, W.; Lifshits, E.; Robinson, H. E.; Katayama, R.; Faber, A. C.; Awad, M. M.; Ramaswamy, S.; Mino-Kenudson, M.; Iafrate, A. J.; Benes, C. H.; Engelman, J. A. Patient-Derived Models of Acquired Resistance Can Identify Effective Drug Combinations for Cancer. *Science* **2014**, *346*, 1480−1486.

(2) Settleman, J. Cancer: Bet on Drug Resistance. *Nature* **2016**, *529*, 289−290.

(3) Obenauf, A. C.; Zou, Y. L.; Ji, A. L.; Vanharanta, S.; Shu, W. P.; Shi, H. B.; Kong, X. J.; Bosenberg, M. C.; Wiesner, T.; Rosen, N.; Lo, R. S.; Massague, J. Therapy-Induced Tumour Secretomes Promote Resistance and Tumour Progression. *Nature* **2015**, *520*, 368−376.

(4) Chen, Q.; Wang, X.; Wang, C.; Feng, L. Z.; Li, Y. G.; Liu, Z. Drug-Induced Self-Assembly of Modified Albumins as Nanotheranostics for Tumor-Targeted Combination Therapy. *ACS Nano* **2015**, *9*, 5223−5233.

(5) Yu, H. J.; Cui, Z. R.; Yu, P. C.; Guo, C. Y.; Feng, B.; Jiang, T. Y.; Wang, S. L.; Yin, Q.; Zhong, D. F.; Yang, X. L.; Zhang, Z. W.; Li, Y. P. pH-and NIR Light-Responsive Micelles with Hyperthermia-Triggered Tumor Penetration and Cytoplasm Drug Release to Reverse Doxorubicin Resistance in Breast Cancer. *Adv. Funct. Mater.* **2015**, *25*, 2489−2500.

(6) Han, N.; Zhao, Q. F.; Wan, L.; Wang, Y.; Gao, Y. K.; Wang, P.; Wang, Z. Y.; Zhang, J. H.; Jiang, T. Y.; Wang, S. L. Hybrid Lipid-Capped Mesoporous Silica for Stimuli-Responsive Drug Release and Overcoming Multidrug Resistance. *ACS Appl. Mater. Interfaces* **2015**, *7*, 3342−3351.

(7) Wang, L.; Lin, X.; Wang, J.; Hu, Z.; Ji, Y.; Hou, S.; Zhao, Y. L.; Wu, X. C.; Chen, C. Y. Novel Insights into Combating Cancer Chemotherapy Resistance Using a Plasmonic Nanocarrier: Enhancing Drug Sensitiveness and Accumulation Simultaneously with Localized Mild Photothermal Stimulus of Femtosecond Pulsed Laser. *Adv. Funct. Mater.* **2014**, *24*, 4229−4239.

(8) Hubbell, J. A.; Chilkoti, A. Nanomaterials for Drug Delivery. *Science* **2012**, *337*, 303−305.

(9) Wei, H.; Zhuo, R. X.; Zhang, X. Z. Design and Development of Polymeric Micelles with Cleavable Links for Intracellular Drug Delivery. *Prog. Polym. Sci.* **2013**, *38*, 503−535.

(10) Meng, H.; Mai, W. X.; Zhang, H. Y.; Xue, M.; Xia, T.; Lin, S. J.; Wang, X.; Zhao, Y.; Ji, Z. X.; Zink, J. I.; Nel, A. E. Codelivery of an Optimal Drug/siRNA Combination Using Mesoporous Silica Nanoparticles to Overcome Drug Resistance in Breast Cancer *in Vitro* and *in Vivo*. *ACS Nano* **2013**, *7*, 994−1005.

(11) He, C. B.; Lu, K. D.; Liu, D. M.; Lin, W. B. Nanoscale Metal-Organic Frameworks for The Co-Delivery of Cisplatin and Pooled siRNAs to Enhance Therapeutic Efficacy in Drug-Resistant Cvarian Cancer Cells. *J. Am. Chem. Soc.* **2014**, *136*, 5181−5184.

(12) Chung, J. E.; Tan, S.; Gao, S. J.; Yongvongsoontorn, N.; Kim, S. H.; Lee, J. H.; Choi, H. S.; Yano, H.; Zhuo, L.; Kurisawa, M.; Ying, J. Y. Self-assembled Micellar Nanocomplexes Comprising Green Tea Catechin Derivatives and Protein Drugs for Cancer Therapy. *Nat. Nanotechnol.* **2014**, *9*, 907−912.

(13) Liu, Y.; Li, L. L.; Qi, G. B.; Chen, X. G.; Wang, H. Dynamic Disordering of Liposomal Cocktails and The Spatio-Temporal Favorable Release of Cargoes to Circumvent Drug Resistance. *Biomaterials* **2014**, *35*, 3406−3415.

(14) Wei, T.; Chen, C.; Liu, J.; Liu, C.; Posocco, P.; Liu, X. X.; Cheng, Q.; Huo, S. D.; Liang, Z. C.; Fermeglia, M.; Pricl, S.; Liang, X. J.; Rocchi, P.; Peng, L. Anticancer Drug Nanomicelles Formed by Self-Assembling Amphiphilic Dendrimer to Combat Cancer Drug Resistance. *Proc. Natl. Acad. Sci. U. S. A.* **2015**, *112*, 2978−2983.

(15) Merino, S.; Martín, C.; Kostarelos, K.; Prato, M.; Vázquez, E. Nanocomposite Hydrogels: 3D Polymer-Nanoparticle Synergies for On-Demand Drug Delivery. *ACS Nano* **2015**, *9*, 4686−4697.

(16) Wang, L. M.; Sun, Q.; Wang, X.; Wen, T.; Yin, J. J.; Wang, P. Y.; Bai, R.; Zhang, X. Q.; Zhang, L. H.; Lu, A. H.; Chen, C. Y. Using Hollow Carbon Nanospheres as a Light-Induced Free Radical Generator to Overcome Chemotherapy Resistance. *J. Am. Chem. Soc.* **2015**, *137*, 1947−1955.

(17) Löscher, W.; Potschka, H. Drug Resistance in Brain Diseases and The Role of Drug Efflux Transporters. *Nat. Rev. Neurosci.* **2005**, *6*, 591−602.

(18) He, Q. J.; Shi, J. L. MSN Anti-Cancer Nanomedicines: Chemotherapy Enhancement, Overcoming of Drug Resistance, and Metastasis Inhibition. *Adv. Mater.* **2014**, *26*, 391−411.

DOI: 10.1021/acsami.6b06522
ACS Appl. Mater. Interfaces 2016, 8, 25060−25068

(19) Guo, X.; Wei, X.; Jing, Y. T.; Zhou, S. B. Size Changeable Nanocarriers with Nuclear Targeting for Effectively Overcoming Multidrug Resistance in Cancer Therapy. *Adv. Mater.* **2015**, *27*, 6450−6456.
(20) Xu, P. S.; Van Kirk, E. A.; Zhan, Y. H.; Murdoch, W. J.; Radosz, M.; Shen, Y. Q. Targeted Charge-Reversal Nanoparticles for Nuclear Drug Delivery. *Angew. Chem., Int. Ed.* **2007**, *46*, 4999−5002.
(21) Qiu, L. P.; Chen, T.; Öcsoy, I.; Yasun, E.; Wu, C. C.; Zhu, G. Z.; You, M. X.; Han, D.; Jiang, J. J. H.; Yu, R. Q.; Tan, W. H. A Cell-Targeted, Size-Photocontrollable, Nuclear-Uptake Nanodrug Delivery System for Drug-Resistant Cancer Therapy. *Nano Lett.* **2015**, *15*, 457−463.
(22) Kroemer, G.; Galluzzi, L.; Brenner, C. Mitochondrial Membrane Permeabilization in Cell Death. *Physiol. Rev.* **2007**, *87*, 99−163.
(23) Ju, E. G.; Li, Z. H.; Liu, Z.; Ren, J. S.; Qu, X. G. Near-Infrared Light-Triggered Drug-Delivery Vehicle for Mitochondria-Targeted Chemo-Photothermal Therapy. *ACS Appl. Mater. Interfaces* **2014**, *6*, 4364−4370.
(24) Biswas, S.; Torchilin, V. P. Nanopreparations for Organelle-Specific Delivery in Cancer. *Adv. Drug Delivery Rev.* **2014**, *66*, 26−41.
(25) Kumar, R.; Han, J.; Lim, H.-J.; Ren, W. X.; Lim, J.-Y.; Kim, J.-H.; Kim, J. S. Mitochondrial Induced and Self-Monitored Intrinsic Apoptosis by Antitumor Theranostic Prodrug: *in Vivo* Imaging and Precise Cancer Treatment. *J. Am. Chem. Soc.* **2014**, *136*, 17836−17843.
(26) Birk, A. V.; Chao, W. M.; Bracken, C.; Warren, J. D.; Szeto, H. H. Targeting Mitochondrial Cardiolipin and The Cytochrome c/Cardiolipin Complex to Ppromote Electron Transport and Optimize Mitochondrial ATP Synthesis. *Br. J. Pharmacol.* **2014**, *171*, 2017−2028.
(27) Gottesman, M. M.; Fojo, T.; Bates, S. E. Multidrug Resistance in Cancer: Role of ATP-Dependent Transporters. *Nat. Rev. Cancer* **2002**, *49*, 48−58.
(28) Holohan, C.; Schaeybroeck, S. V.; Longley, D. B.; Johnston, P. G. Cancer Drug Resistance: an Evolving Paradigm. *Nat. Rev. Cancer* **2013**, *13*, 714−726.
(29) Han, K.; Liu, Y.; Yin, W. N.; Wang, S. B.; Xu, Q.; Zhuo, R. X.; Zhang, X. Z. A FRET-Based Dual-Targeting Theranostic Chimeric Peptide for Tumor Therapy and Real-Time Apoptosis Imaging. *Adv. Healthcare Mater.* **2014**, *3*, 1765−1768.
(30) Han, K.; Zhang, W. Y.; Zhang, J.; Lei, Q.; Wang, S. B.; Liu, J. W.; Zhang, X. Z.; Han, H. Y. Acidity-Triggered Tumor-Targeted Chimeric Peptide for Enhanced Intra-Nuclear Photodynamic Therapy. *Adv. Funct. Mater.* **2016**, *26*, 4351−4361.
(31) Li, S. Y.; Liu, L. H.; Cheng, H.; Li, B.; Qiu, W. X.; Zhang, X. Z. A Dual-FRET-based Fluorescence Probe for The Sequential Detection of MMP-2 and Caspase-3. *Chem. Commun.* **2015**, *51*, 14520−14523.
(32) Han, K.; Wang, S. B.; Lei, Q.; Zhu, J. Y.; Zhang, X. Z. Ratiometric Biosensor for Aggregation-Induced Emission-Guided Precise Photodynamic Therapy. *ACS Nano* **2015**, *9*, 10268−10277.
(33) Chen, J. X.; Wang, H. Y.; Li, C.; Han, K.; Zhang, X. Z.; Zhuo, R. X. Construction of Surfactant-Like Tetra-Tail Amphiphilic Peptide with RGD Ligand for Encapsulation of Porphyrin for Photodynamic Therapy. *Biomaterials* **2011**, *32*, 1678−1684.
(34) Han, K.; Lei, Q.; Jia, H. Z.; Wang, S. B.; Yin, W. N.; Chen, W. H.; Cheng, S. X.; Zhang, X. Z. A Tumor Targeted Chimeric Peptide for Synergistic Endosomal Escape and Therapy by Dual-Stage Light Manipulation. *Adv. Funct. Mater.* **2015**, *25*, 1248−1257.
(35) Tsai, H. C.; Imae, T.; Calderó, G.; Solans, C. Two-Photon Confocal Imaging Study: Cell Uptake of Two Photon Dyes-Labeled PAMAM Dendrons in HeLa Cells. *J. Biomed. Mater. Res., Part A* **2012**, *100A*, 746−756.
(36) Han, K.; Lei, Q.; Wang, S. B.; Hu, J. J.; Qiu, W. X.; Zhu, J. Y.; Yin, W. N.; Luo, X.; Zhang, X. Z. Dual-Stage-Light-Guided Tumor Inhibition by Mitochondria-Targeted Photodynamic Therapy. *Adv. Funct. Mater.* **2015**, *25*, 2961−2971.
(37) Okada, M.; Smith, N. I.; Palonpon, A. F.; Endo, H.; Kawata, S.; Sodeoka, M.; Fujita, K. Label-Free Raman Observation of Cytochrome c Dynamics During Apoptosis. *Proc. Natl. Acad. Sci. U. S. A.* **2012**, *109*, 28−32.
(38) Standley, S. M.; Toft, D. J.; Cheng, H.; Soukasene, S.; Chen, J.; Raja, S. M.; Band, V.; Band, H.; Cryns, V. L.; Stupp, S. I. Induction of Cancer Cell Death by Self-Assembling Nanostructures Incorporating a Cytotoxic Peptide. *Cancer Res.* **2010**, *70*, 3020−3026.
(39) Liu, S. Q.; Tong, Y. W.; Yang, Y. Y. Thermally Sensitive Micelles Self-Assembled from Poly(N-isopropylacrylamide-co-N,N-dimethylacrylamide)-b-Poly(d,l-lactide-co-glycolide) for Controlled Delivery of Paclitaxel. *Mol. BioSyst.* **2005**, *1*, 158−165.
(40) Rainbolt, E. A.; Miller, J. B.; Washington, K. E.; Senevirathne, S. A.; Biewer, M. C.; Siegwart, D. J.; Stefan, M. C. Fine-Tuning Thermoresponsive Functional Poly(ε-caprolactone)s to Enhance Micelle Stability and Drug Loading. *J. Mater. Chem. B* **2015**, *3*, 1779−1787.
(41) Jiang, L.; Li, L.; He, X.; Yi, Q. Y.; He, B.; Cao, J.; Pan, W. S.; Gu, Z. W. Overcoming Drug-Resistant Lung Cancer by Paclitaxel Loaded Dual-Functional Liposomes with Mitochondria Targeting and pH-Response. *Biomaterials* **2015**, *52*, 126−139.
(42) Chou, T. C. Drug Combination Studies and Their Synergy Quantification using the Chou-Talalay Method. *Cancer Res.* **2010**, *70*, 440−448.
(43) Gottesman, M. M. Mechanisms of Cancer Drug Resistance. *Annu. Rev. Med.* **2002**, *53*, 615−627.
(44) Zhou, J.; Du, X. W.; Yamagata, N.; Xu, B. Enzyme-Instructed Self-Assembly of Small d-Peptides as a Multiple-Step Process for Selectively Killing Cancer Cells. *J. Am. Chem. Soc.* **2016**, *138*, 3813−3823.
(45) Li, Y.; Deng, Y.; Tian, X.; Ke, H.; Guo, M.; Zhu, A.; Yang, T.; Guo, Z. Q.; Ge, Z. S.; Yan, X. L.; Chen, H. B. Multipronged Design of Light-Triggered Nanoparticles to Overcome Cisplatin Resistance for Efficient Ablation of Resistant Tumor. *ACS Nano* **2015**, *9*, 9626−9637.

DOI: 10.1021/acsami.6b06522
ACS Appl. Mater. Interfaces 2016, 8, 25060−25068